

A Novel Gold Nanorod-based HR1 Peptide Inhibitor for Middle East Respiratory Syndrome Coronavirus

Xinyu Huang, Meng Li, Yurui Xu, Jikang Zhang, Xia Meng, Xueying An, Lei Sun, Leilei Guo, Xue Shan, Junliang Ge, Jiao Chen, Yadong Luo, Heming Wu, Yu Zhang, Qing Jiang, and Xinghai Ning

ACS Appl. Mater. Interfaces, **Just Accepted Manuscript** • DOI: 10.1021/acsami.9b04240 • Publication Date (Web): 17 May 2019

Downloaded from <http://pubs.acs.org> on May 19, 2019

Just Accepted

“Just Accepted” manuscripts have been peer-reviewed and accepted for publication. They are posted online prior to technical editing, formatting for publication and author proofing. The American Chemical Society provides “Just Accepted” as a service to the research community to expedite the dissemination of scientific material as soon as possible after acceptance. “Just Accepted” manuscripts appear in full in PDF format accompanied by an HTML abstract. “Just Accepted” manuscripts have been fully peer reviewed, but should not be considered the official version of record. They are citable by the Digital Object Identifier (DOI®). “Just Accepted” is an optional service offered to authors. Therefore, the “Just Accepted” Web site may not include all articles that will be published in the journal. After a manuscript is technically edited and formatted, it will be removed from the “Just Accepted” Web site and published as an ASAP article. Note that technical editing may introduce minor changes to the manuscript text and/or graphics which could affect content, and all legal disclaimers and ethical guidelines that apply to the journal pertain. ACS cannot be held responsible for errors or consequences arising from the use of information contained in these “Just Accepted” manuscripts.



A Novel Gold Nanorod-based HR1 Peptide Inhibitor for Middle East Respiratory Syndrome Coronavirus

Xinyu Huang,^{a#} Meng Li,^{b#} Yurui Xu,^a Jikang Zhang,^a Xia Meng,^a Xueying An,^c Lei Sun,^a Leilei Guo,^d Xue Shan,^a Junliang Ge,^a Jiao Chen,^e Yadong Luo,^b Heming Wu,^b Yu Zhang,^{ a} Qing Jiang,^{*c} and Xinghai Ning^{*a}*

^a Nanjing National Laboratory of Microstructures, College of Engineering and Applied Sciences, Nanjing University, Nanjing 210093, China

^b Jiangsu Key Laboratory of Oral Diseases, Nanjing Medical University, Nanjing 210029, China

^c State Key Laboratory of Pharmaceutical Biotechnology, Department of Sports Medicine and Adult Reconstructive Surgery, Nanjing Drum Tower Hospital, The Affiliated Hospital of Nanjing University Medical School, Nanjing 210008, China

^d State Key Laboratory of Natural Medicines, China Pharmaceutical University, Nanjing 210009, China

^e Jiangsu Province Academy of Traditional Chinese Medicine, Nanjing 210028, China

These authors contributed equally to this work.

1
2
3 KEYWORDS: gold nanorods, peptides, inhibitors, viral infections, MERS
4
5

6
7 ABSTRACT: Middle East respiratory syndrome coronavirus (MERS-CoV) causes a SARS-like
8
9 illness with high pathogenicity and mortality due to the lack of effective therapeutics. Currently,
10
11 only few antiviral agents are available for the treatment of MERS, but their effects have been
12
13 greatly impaired by low antiviral activity, poor metabolic stability and serious adverse effect.
14
15 Therefore, the development of effective treatment for MERS is urgently needed. In this study, a
16
17 series of HR1 peptide inhibitors have been developed to inhibit HR1/HR2-mediated membrane
18
19 fusion between MERS-CoV and host cells, which is the major pathway of MERS-CoV-induced
20
21 host infections. Particularly, peptide PIH exhibits potent inhibitory activity with IC_{50} of 1.171
22
23 μM , and its inhibitory effects can be further increased to ten-fold by forming the gold nanorod
24
25 complex (PIH-AuNRs). In addition, PIH-AuNRs display enhanced metabolic stability and
26
27 biocompatibility *in vitro* and *in vivo*, and therefore effectively prevent MERS-CoV-associated
28
29 membrane fusion. In summary, PIH-AuNRs represent a novel class of antiviral agents, and have
30
31 the great potential of treating MERS in the clinic.
32
33
34
35
36
37

38 **Introduction**

39
40

41 Middle East respiratory syndrome coronavirus (MERS-CoV) has been identified as an infective
42
43 virus¹ with high pathogenicity^{2, 3} and mortality rate⁴. MERS-CoV can cause severe respiratory
44
45 illnesses,⁵ and is recognized as a serious threat to public health.⁶ Currently, there has been no
46
47 vaccine or effective treatment for MERS,⁷ which mainly relies on supportive treatment and the
48
49 combination therapy of traditional antiviral drugs, such as interferon and ritonavir. However,
50
51 neither of them showed good antiviral effects on the patients, leading to limited therapeutic
52
53
54
55
56
57
58
59
60

1
2
3 applications.⁸⁻¹⁰ Therefore, there is an urgent need for developing effective therapeutics for
4
5 MERS.
6

7
8 A growing number of evidences show that MERS-CoV infections were caused by Spike protein
9 (S protein)-mediated membrane fusion between MERS-CoV and host cells.¹¹ S protein is a type I
10 transmembrane glycoprotein expressed as a trimer on the surface of the viral envelope, and plays
11 a critical role in MERS infections.¹² S protein contains two functional subunits, S1 and S2. S1
12 protein is responsible for binding host cells through recognizing dipeptidyl peptidase 4 receptors
13 (DPP4),¹³ and consequently trigger S2 protein to mediate the fusion of MERS-CoV envelope
14 with host cell membrane. The critical roles of S2 protein in regulating MERS-CoV infections
15 indicate that inhibition of S2 protein function is a potent approach for MERS treatment. The S2
16 protein consists of three major domains, HR1 (heptad repeat 1), HR2 (heptad repeat 2) and
17 fusion peptides (FP). When S1 binds to the dipeptidyl peptidase 4 receptor (DPP4), the FP
18 inserts into the host cell membrane, and then the HR1 triplex and the HR2 triplex bind to each
19 other to form a 6-helix bundle (6-HB).¹⁴ The 6-HB draws the MERS-CoV envelope and the host
20 cell membrane toward each other, and promotes their fusion, leading to the release of the viral
21 genetic RNA into host cells (Figure 1). Therefore, the formation of 6-HB plays a key role in
22 mediating the fusion of the MERS-CoV envelope with the target cell membrane, making it a
23 good target for preventing MERS-CoV infections.
24
25
26
27
28
29
30
31
32
33
34
35
36
37
38
39
40
41
42
43
44
45

46 In this study, we have developed a series of peptide inhibitors, based on the crystal structure of
47 6-HB formed by the interaction of HR1 and HR2 domains (PDB ID: 4NJL). Peptide inhibitors
48 were designed using the docking-based virtual screening method, on the basis of the HR2
49 sequence. We identified an α -helix peptide, named PIH, which could mimic the conformation of
50 HR2, and selectively interact with HR1 to block the formation of 6-HB. PIH showed good
51
52
53
54
55
56
57
58
59
60

1
2
3 inhibitory activity against the S protein-mediated membrane fusion; particularly, PIH-modified
4 gold nanorods (PIH-AuNRs) showed enhanced inhibitory activity. In addition, PIH-AuNR with
5 improved biostability and biocompatibility, had better physical and pharmaceutical profile than
6 PIH alone, endowing potential clinical applications. Therefore, PIH-AuNRs hold the great
7 potential for the treatment of Middle East Respiratory Syndrome Coronavirus.
8
9

15 **Experimental Section**

16
17
18
19 **Materials and Instrument.** All chemicals and solvents are of reagent grade unless otherwise
20 indicated. All chemicals were purchased from Sigma and Aladdin Reagent Company without
21 further purification. HR1 was purchased from KareBay Biochem Company. Cell Counting Kit-8
22 (CCK-8) was purchased from Beyotime. 293T cell line and Huh-7 cell line were obtained from
23 Cell Bank of Chinese Academy of Science. 293T and Huh-7 cell lines were cultured in
24 Dulbecco's Modified Eagle Medium (DMEM) (Invitrogen) supplemented with 10% fetal bovine
25 serum (FBS) (Gibco) and penicillin/streptomycin (1%, w/v). ICR female mice were purchased
26 from Nanjing Qinglongshan Experimental Animal Center. Mice used in experiments were 8–10
27 weeks old. All procedures were approved by Affiliated Drum Tower Hospital of Nanjing
28 University Medical School Ethics Committee and carried out in accordance with the National
29 Institute of Health Guide for the Care and Use of Laboratory Animals.
30
31
32
33
34
35
36
37
38
39
40
41
42
43
44

45 Peptide synthesis was performed on an automated peptide synthesizer (Multisyntech). High-
46 performance liquid chromatography (HPLC, Shimadzu) was used for peptide purification and
47 serum stability study. MS were acquired from the NJU Mass Spectral Facility using electrospray
48 ionization (ESI-TOF). Circular dichroism (CD) spectroscopy analysis was performed on a J-815
49 spectropolarimeter (Jasco). Fluorescence images were taken by an inverted fluorescence
50
51
52
53
54
55
56
57
58
59
60

1
2
3 microscope (Nikon Instruments). Cytotoxicity assays were performed on a microplate reader
4
5 (Tecan Group). Transmission electron microscope (TEM) images were taken with an H-800
6
7 transmission electron microscope (Hitachi). Dynamic light scattering (DLS) was performed on a
8
9 Zetasizer Nano ZS (Malvern). UV-Vis spectra were measured on JINGHUA UV-1800
10
11 spectrophotometer.
12
13

14
15 **Design of HR1 peptide inhibitors.** The 3D structure of the peptides were modeled based on the
16
17 template of the HR2 helix of MERS-CoV fusion core (PDB ID: 4NJL), using the Accelrys
18
19 Discovery Studio 4.1 software. The best homology model was refined by restrained energy
20
21 minimization with adopting the OPLS3 force field. The heavy atoms were converged to RMSD
22
23 of 2.0 Å. Then the peptides were docked with the HR1 helices of MERS-CoV fusion core using
24
25 Schrodinger 2015-3. The binding energies of the peptides with HR1 core helices of MERS-CoV
26
27 were estimated by MM-GBSA method using VSGB solvation model in OPLS3 force field.
28
29 Interactions between the peptides and HR1 core helices of MERS-CoV were viewed in PyMOL
30
31
32 1.7.4. The peptide with highest binding energy was chosen for further inhibition studies.
33
34
35

36
37 **Synthesis of PIH.** PIH was synthesized with the standard solid-phase procedure,¹⁵ purified by
38
39 HPLC and identified by LC-ESI-MS. VP-ODS C18 column (150 × 4.6 mm, 5 μm) was used for
40
41 HPLC analyses. The solvent A (0.1% TFA in 100% water (v/v)) and the solvent B (0.1% TFA in
42
43 80% acetonitrile and 20% water (v/v)) were chosen as mobile phases. The flow rate was
44
45 1mL/minute, and the flow gradient from 50% to 75% solvent B was performed during 20
46
47 minutes.
48
49
50

51
52 **Circular dichroism (CD) spectroscopy analysis.** The secondary structure of PIH was
53
54 determined by circular dichroism analysis. The PIH was dissolved in PBS (pH 7.2), and the CD
55
56
57
58
59
60

1
2
3 spectra were measured on a J-815 spectropolarimeter at 20°C with a parameter set of 1.0 nm
4 bandwidth in the range of 190 to 260 nm, 0.1 nm resolution, 100 μm path length, 4-second
5 response time, and a 50 nm/minute scanning speed. The absorbance of PBS was subtracted to
6 calibrate the spectra of PIH.
7
8
9
10
11

12
13 **Sodium dodecyl sulphate polyacrylamide gel electrophoresis (SDS–PAGE).** SDS–PAGE was
14 performed to measure the formation of 6-HB with HR1 (KareBay) and PIH.^{16,17} HR1 (10 mM),
15 PIH (10 mM) and their mixture (25 mM, HR1: PIH= 1: 1), were incubated in PBS at room
16 temperature for 30 minutes. All samples were diluted with loading buffer, loaded onto the gel,
17 and run at 120 V for 60 minutes, until the tracking dye reached the bottom edge of the gel. The
18 gel was then stained and imaged with Coomassie blue.
19
20
21
22
23
24
25
26
27

28 **Serum stability.** Enzymatic degradation studies were carried out using 100% fetal calf serum.
29 PIH solution (20 μL, 10 mM in PBS) was added to serum (380 μL), and was incubated at 37°C
30 for 12 hours. The cultured mixtures (20 μL) were taken at different time points (0, 0.2, 0.5, 1, 2,
31 4, 6, 8 or 12 hour), and the samples were added glacial acetonitrile (90 μL), vortexed, and
32 maintained in ice bath for 5 minutes. Then, samples were diluted with acetic acid (90 μL, 0.5%,
33 v/v) and centrifuged at 10, 000 g for 15 minutes. The supernatants were collected for RP-HPLC
34 analysis. The process of peptide degradation conforms to the first-order kinetic equation: $A_t = A_0 e^{-kt}$.
35 The degradation half-life ($t_{1/2}$) of PIH was calculated by using the IBM SPSS software.
36
37
38
39
40
41
42
43
44
45
46
47

48 **MERS-CoV S2 subunit-mediated cell fusion model.** 293T cells were transfected with the
49 plasmid of either pAAV-IRES-MERS-EGFP or pAAV-IRES-EGFP, and cultured at 37°C for 36
50 hours, generating 293T/MERS/EGFP and 293T/EGFP, respectively. Huh-7 cells (5×10^4) were
51 incubated in 96-well microplates at 37°C for 12 hours, followed by adding 2×10^4 293T/EGFP or
52
53
54
55
56
57
58
59
60

1
2
3 293T/MERS/EGFP cells. The cell fusion was imaged using an inverted fluorescence microscope
4
5 at different time points (0, 1, 2, 3, 4, 5, 6, 8, 12 hour). The fused cells were identified by
6
7 measuring EGFP fluorescence intensity, which is at least one-fold lower in fused cells than intact
8
9 cells. The numbers of cell fusion were calculated using the Image J software. The fusion rates
10
11 (F) were calculated using the following formula: $N/T \times 100\%$. ' N ' represents the numbers of fused
12
13 cells; ' T ' represents the total numbers of 293T cells.
14
15
16
17

18 **Inhibition of MERS-CoV S2 subunit-mediated cell fusion.** 293T/MERS/EGFP or 293T/EGFP
19
20 cells (2×10^4) were pre-treated with HR1 inhibitors for 30 minutes, and then added into Huh-7
21
22 cells (5×10^4). After co-culture at 37°C for 6 hours, cell fusions were imaged using a fluorescence
23
24 microscope. The numbers of cell fusion were calculated using the Image J software. The fusion
25
26 rates (F_P , F_H , F_N) were calculated using the following formula: $F/A \times 100\%$. ' F ' represents the
27
28 numbers of fused cells; ' A ' represents the total numbers of 293T cells; ' F_P ' represents the cell
29
30 fusion rate between 293T/MERS/EGFP and Huh-7 cells in absence of HR1 inhibitors; ' F_H '
31
32 represents the cell fusion rate between 293T/MERS/EGFP cells and Huh-7 cells in the presence
33
34 of HR1 inhibitors; ' F_N ' represents the cell fusion rate of between 293T/EGFP cells and Huh-7
35
36 cells in absence of HR1 inhibitors. The inhibition rate (I) of cell fusions was calculated using the
37
38 following formula: $(F_P - F_H)/(F_P - F_N) \times 100\%$. The concentration for 50% inhibition (IC_{50}) was
39
40 calculated using the IBM SPSS software.
41
42
43
44
45
46

47 **Cytotoxicity assay.** The cytotoxicity was evaluated with a CCK-8 kit. Huh-7, 293T and L02
48
49 cells (5×10^3 cells) were seeded into 96-well microplates, and cultured at 37°C overnight. Cells
50
51 were incubated with different concentrations of HR1 inhibitors for 48 hours, followed by adding
52
53
54
55
56
57
58
59
60

1
2
3 CCK-8 solution (10 μ L). The absorbance at 570 nm was read on a microplate reader after 2-hour
4
5 incubation.
6
7

8
9 **The preparation and characterization of PIH-AuNRs.** PIH (8 μ L, 1.3 mM) was added into
10 the solution of excess AuNRs (2.0 mL, 3.4 nM) with a molar ratio of 1500: 1 between PIH and
11 AuNRs. After 12-hour stirring, the reaction mixture was filtrated (pore size, 0.22 μ m) and
12
13 centrifuged, and the supernatant was analyzed by HPLC to evaluate the conjugation yield. HPLC
14
15 data showed that that all PIH was successfully immobilized on AuNRs, generating PIH-modified
16
17 AuNRs, which has about 1529 PIH on single AuNR. Then, PIH-modified AuNRs were further
18
19 coated with HS-PEG2000-COOH (2.0 mL, 100 μ M) for 12 hours, and PIH-AuNRs were
20
21 collected by centrifugation at 10, 000 rpm for 15 minutes, and washed by PBS buffer for twice.
22
23 The final PIH-AuNRs were resuspended in PBS buffer, and stored at 4 $^{\circ}$ C . PIH-AuNRs was
24
25 characterized with TEM. The zeta potential of PIH-AuNRs was measured by DLS with a
26
27 scattering angle 90 $^{\circ}$ at 25 $^{\circ}$ C.
28
29
30
31
32
33
34

35
36 **Biochemical parameters.** ICR mice were injected with PIH-AuNRs (20 mg kg $^{-1}$) or saline via
37 the tail vein every 3 days for 12 days. At day 12, mice were sacrificed, and the serum was
38
39 collected for biochemical studies. ALT, AST, TBIL, TNF- α , Il-1 β and Il-6 were measured using
40
41 ELISA assays.
42
43
44

45
46 **Histopathology studies.** ICR mice, treated with PIH-AuNRs (20 mg kg $^{-1}$) or saline for 12 days,
47
48 were sacrificed, and various organs were harvested, embedded in the paraffin, and stained with
49
50 hematoxylin and eosin (H&E). The images were captured using inverted microscope.
51
52
53
54
55
56
57
58
59
60

1
2
3 **Statistics.** All experiments were repeated at least 3 times with 6-12 biological replicates. Error
4 bars represent standard error of the mean from independent samples assayed within the
5 experiments. Statistical analysis was done with GraphPad Prism 6 software. Statistical
6 significance was calculated using unpaired Student's t-test, and a p-value<0.05 was considered to
7 be statistically significant.
8
9

10 **Results and Discussion**

11
12 **Molecular design of PIH.** The amino-acid sequence of MERS-CoV S protein (GenBank:
13 JX869059.1) was obtained from NCBI, containing HR1 domain (residues 984–1,104) and HR2
14 domain (residues 1,246–1,295) (Figure 2a). Based on the interaction model between HR1 and
15 HR2 in 6-HB, we have designed a series of peptide inhibitors, which mimic the HR2 helix
16 conformation (Table S1). After mimetic screening, we obtained a peptide inhibitor, named PIH,
17 which showed the highest binding affinity for HR1. PIH shared 65% identity with the HR2 helix
18 (PDB ID: 4NJL) with nine modified amino acids, and had the highest docking score of -365.882
19 kcal mol⁻¹ (Figure 2b), indicating that PIH is a promising HR1 inhibitor. We constructed the 3D
20 structure of PIH based on HR2 helix using homology modelling of Discovery Studio 4.1
21 software. As shown in Figure 2c, PIH has a regular α -helix in the middle region and random
22 coils at the N- and C-terminals. Docking studies showed that PIH and HR1 helix could form the
23 6-HB analog through hydrophobic and hydrophilic interactions (Figure 2d and 2e), which is
24 consistent with the interaction between HR1 and HR2 helix in MERS-CoV fusion core.
25
26

27
28
29
30
31
32
33
34
35
36
37
38
39
40
41
42
43
44
45
46
47
48
49
50
51
52
53
54
55
56
57
58
59
60
PIH interacted with hydrophobic grooves formed between two adjacent HR1 helices mainly
through hydrophobic interactions, involving N-terminal portion (L2, I5, L9, L10), α -helix
portion (L12, M16, L19, V22, V23, L26), and C-terminal portion (Y30, I31, L33 and L36) of

1
2
3
4
5
6
7
8
9
10
11
12
13
14
15
16
17
18
19
20
21
22
23
24
25
26
27
28
29
30
31
32
33
34
35
36
37
38
39
40
41
42
43
44
45
46
47
48
49
50
51
52
53
54
55
56
57
58
59
60

PIH (Figure 2d). In addition, PIH also interacted with HR1 hydrophilic regions by hydrogen bonds. For example, the N-terminal portion (S1, T3, E8, L10, D11, L12) of PIH formed eight hydrogen bonds with one HR1 helix (G1250, E1039, K1035, N1028, K1021) and the adjacent HR1 helix (N1027, Q1023); the α -helix portion (E13, E15, M16, V23, K25, E27, E28, S29) of PIH formed seven hydrogen bonds with one HR1 helix (K1021, T1010, K1000) and the adjacent HR1 helix (Q1023, N1016, Q1009); the C-terminal portion (Y30, I31, L36) of PIH formed five hydrogen bonds with one HR1 helix (K1000, N993) and the adjacent HR1 helix (N1002, Q1009). Therefore, PIH was tightly bound to HR1 through the hydrophobic and hydrophilic interactions, and competitively inhibited the formation of 6-HB, indicating that PIH is a potent inhibitor against MERS-CoV infections.

Biophysical characterization of PIH. We synthesized PIH and fully characterized its biophysical and biological properties. PIH was synthesized by the solid phase synthetic method, and characterized by LC-MS (Figure 3a and Figure S1). PIH spontaneously formed α -helix in PBS, which was confirmed by circular-dichroism spectroscopy (Figure 3b). As expected, PIH has two negative absorption (208, 222 nm), indicating that it forms α -helix structure.

We proposed that inhibiting the formation of 6-HB between HR1 and HR2 is an effective method to prevent MERS-CoV infections. We therefore investigated whether PIH could form the complex with HR1. Sodium dodecyl sulfate–polyacrylamide gel electrophoresis (SDS-PAGE) analysis showed that a new band of \sim 26 kDa was observed in the mixture of PIH and HR1 (Figure 3c), which matches the molecular mass of a 6-HB formed by HR1 (\sim 4 kDa) and PIH (\sim 4 kDa), which is consistent with native polyacrylamide-gel electrophoresis (N-PAGE) analysis (Figure S2). Therefore, PIH interacts with HR1 to form 6-HB, and is a promising HR1 inhibitor.

1
2
3 **Serum stability of PIH.** Peptide drugs have been recognized as ideal therapeutics for critical
4 diseases in the clinic due to good biocompatibility, specificity and efficacy.¹⁸ However, their
5 clinical potential has been hindered by their low stability and bioavailability. Particularly, protein
6 kinases randomly decompose peptide drugs, and consequently minimize their *in vivo* potency.
7
8 Therefore, we evaluated the stability of PIH in the fetal calf serum, and its half-life was
9 calculated. As shown in Figure 3d, PIH displayed good metabolic stability in serum with the $t_{1/2}$
10 of 6.93 hours, indicating that it is a potent drug candidate for *in vivo* applications.
11
12
13
14
15
16
17
18
19

20 **PIH-induced inhibition of S2 subunit-mediated cell fusion.** MERS-CoV infects host cells
21 through S2 subunit-induced membrane fusion. During infections, HR1 and HR2 domains in S2
22 subunit form a 6-HB fusion core, which is responsive for membrane fusion between MERS-CoV
23 and host cells. Therefore, inhibiting the formation of 6-HB is a promising method against
24 MERS-CoV infections. However, MERS-CoV belongs to a family of viruses that can infect a
25 variety of mammalian hosts, and is readily transmissible among humans by direct contact with
26 respiratory secretions, body fluids and excretions from infected individuals. Consequently, the
27 containment level 3 is required for all *in vitro* and *in vivo* studies, significantly hindering the
28 development of anti-MERS treatments. We therefore constructed the cell fusion model to
29 systemically evaluate therapeutic efficacy of anti-MERS agents.
30
31
32
33
34
35
36
37
38
39
40
41
42
43

44 It has been reported that Huh-7 cells showed higher susceptibility to MERS-CoV than respiratory
45 tract cells,¹⁹ and therefore, we have constructed the cell fusion model with 293T cells co-expressed
46 with EGFP/S protein and Huh-7 cells with MERS-CoV receptor DPP4.²⁰ We thus performed
47 experiments to verify whether PIH could inhibit cell fusion mediated by S2 subunit. The cellular
48 size of 293T cells (MERS/EGFP) increased after fusing with Huh-7 cells, and fused cells showed
49 at least two-fold lower fluorescence intensity, compared to 293T cells (EGFP) (Figure 4a),
50
51
52
53
54
55
56
57
58
59
60

1
2
3 indicating that S proteins on the 293T cells could recognize DPP4 on Huh-7 cells to induce cell
4 fusion. In addition, we further identified that cell fusion between 293T and Huh-7 cells showed
5 time-dependence, and reached the plateau after six hours (Figure 4b). Based on this established
6 cell fusion model, we further investigated the inhibitory effects of PIH on S2 subunit-mediated
7 cell fusion at six hours after co-culture. Figures 4c and 4d show that PIH had a dose-dependent
8 responding profile with IC_{50} of 1.171 μM , and could completely inhibit the cell fusion at a
9 concentration of 10 μM , indicating that PIH has a high inhibitory activity for MERS-CoV
10 infections.
11
12
13
14
15
16
17
18
19
20
21

22 **Cytotoxicity of PIH.** Peptide-based therapeutics have been recognized as ideal drug candidates
23 due to their high selectivity, biocompatibility and potency. However, some peptide drug
24 candidates failed in the clinical trials due to unexpected cytotoxicity.²¹ We therefore assessed
25 cytotoxicity of PIH on 293T, Huh-7 and L02 cells. As shown in Figure 4e, PIH displayed no
26 significant cytotoxicity to mammalian cells even at a high concentration of 100 μM , which is
27 ten-fold higher than the concentration needed for fully inhibiting cell fusion. The selectivity
28 index ($SI=CC_{50}/IC_{50}$) of PIH is 132, suggesting that PIH is an effective MERS-CoV inhibitor
29 with no adverse effects.
30
31
32
33
34
35
36
37
38
39
40
41

42 **The preparation and characterization of PIH-AuNRs.** Although PIH exhibited significant
43 inhibitory activity, peptides along suffer major drawbacks, such as poor metabolic stability and
44 bioavailability.²² The construction of conjugates between peptides and gold nano-cargos
45 represents a promising strategy for improving their pharmacokinetics and pharmacodynamics.
46 There are many types gold nanostructures, such as gold nanoparticles, nanorods (AuNRs),
47 nanoplates, nanodisks and nanoshells, and all of them have been widely used in the diagnosis and
48 treatment of various diseases due to their unique physical and chemical properties. Particularly,
49
50
51
52
53
54
55
56
57
58
59
60

1
2
3 AuNRs have been widely used in biomedical applications, and especially theranostic and thermo-
4 chemotherapeutic applications.²³⁻²⁵ For example, AuNRs are a promising nanosized drug delivery
5 system, and can effectively deliver drugs in diseased tissues, thereby greatly improving therapeutic
6 efficacy. In addition, AuNRs have tunable surface plasmon and photothermal effects, endowing
7 them with good photoacoustic and photothermal effects. Furthermore, AuNRs, as a nanocarrier for
8 chemotherapeutic agents, can provide effective combined chemo-photothermal therapy. Most
9 importantly, the surface of AuNRs can be easily modified with biocompatible materials, making
10 them an ideal drug delivery platform.
11
12
13
14
15
16
17
18
19
20
21

22
23 In recent years, AuNRs have been identified as potential biocompatible and site-specific carriers
24 for antiviral theranostic agents. For example, AuNRs-mediated delivery of ssRNA was developed
25 as a unique therapeutics for the treatment of seasonal and pandemic flu.²³ These findings suggest
26 that AuNRs-based antiviral agents represent a promising approach for the management of infectious
27 diseases. Therefore, we developed PIH-modified gold nanorods (PIH-AuNRs) with polyethylene
28 glycol (PEG) coating (Figure 5a). The PEG coating on AuNRs could not only enhance the
29 stability and hydrophilicity of PIH-AuNRs by reducing nonspecific binding of proteins,²⁶ but
30 minimize the phagocytic clearance by the reticuloendothelial system (RES) *in vivo*,^{27, 28} leading
31 to improving pharmacokinetic and pharmacodynamics properties.
32
33
34
35
36
37
38
39
40
41
42
43

44 PIH has a cysteine residue with a free thiol moiety at the N-terminus, and can be immobilized on
45 AuNRs by the Au-S chelation. PIH and AuNRs were mixed for 12 hours, and the reaction mixture
46 was filtrated and centrifuged. The supernatant of the reaction mixture was analyzed by HPLC to
47 evaluate the conjugation yield of PIH. Figure S6 shows that all PIH was successfully immobilized
48 on AuNRs. In addition, we performed TEM to identify the morphology of PIH-AuNRs, which
49 were in the nano-range with a length of 54.2 ± 1.3 nm and a diameter of 18.0 ± 0.7 nm (Figure
50
51
52
53
54
55
56
57
58
59
60

1
2
3 5b). The zeta potential of AuNRs was 36.9 mV, and changed to -16.9 mV and -34.9 mV after
4
5
6
7
8
9
10
11
12
13
14
15
16
17
18
19
20
21
22
23
24
25
26
27
28
29
30
31
32
33
34
35
36
37
38
39
40
41
42
43
44
45
46
47
48
49
50
51
52
53
54
55
56
57
58
59
60

PIH and PEG modification, respectively, indicating that PIH-AuNRs were successfully prepared (Figure 5c). In addition, the UV-Vis spectra of PIH-AuNRs showed a red shift absorption, compared to AuNRs (Figure 5d), further confirming the formation of PIH-AuNRs.

Biological evaluation of PIH-AuNRs. We further assessed the inhibitory activity of PIH-AuNRs using the cell fusion model. Figures 5e and 5f show that PIH-AuNRs showed a higher inhibitory activity than PIH, partially due to multivalent effects. For example, PIH-AuNRs could completely inhibit cell fusion at the concentration of 1.0 μM , and had ten-fold higher inhibitory activity than peptide PIH. In addition, PIH displayed good biocompatibility, and did not affect cell viability on 293T, Huh-7 and L02 cells (Figure 5g), indicating that PIH-AuNRs are a more potent anti-MERS agent than peptide PIH.

Biostability and biosafety of PIH-AuNRs. Peptide-modified AuNRs have some critical issues for *in vivo* applications due to limited pharmacokinetics and pharmacodynamics.²⁹ Therefore, we further assessed the biostability and biosafety of PIH-AuNRs *in vitro* and *in vivo*, and identified their clinical application prospects. Figure 6a shows that PIH-AuNRs exhibited strong inhibitory activity after 12-hour incubation in serum, and could inhibit more than 90% of cell fusion at the concentration of 1.171 μM . In contrast, PIH lost inhibitory effects after 12-hour incubation in serum, indicating that the conjugation of AuNRs can greatly improve biostability of PIH. In addition, PEG modification could further enhance the biostability and bioavailability of PIH-AuNRs *in vivo*.³⁰

To further assess the possibility of *in vivo* applications of PIH-AuNRs, we evaluated their biocompatibility in ICR mice. Mice were administrated intravenously with either PIH-AuNRs

1
2
3 (100 mg kg⁻¹) or saline (control) every 3 days for 12 days. Figure 6b shows that the body weights
4 of mice gradually increased, and no significant differences were observed between the PIH-
5 AuNRs and control groups at any given time points. In addition, no apparent signs of
6 dehydration, behavioral abnormalities and other symptoms related to systemically toxic effects
7 were observed during the treatment, suggesting PIH-AuNRs are a biosafe AuNR-based
8 therapeutics.
9

10
11
12 **Biochemical parameters and histopathology.** Normally, hepatotoxicity is a major hindrance
13 for clinical applications of nanoparticle-based therapeutics due to nonspecific liver
14 accumulation.^{31, 32} We therefore performed experiments to investigate PIH-AuNRs induced
15 adverse effects by measuring biochemical parameters and histopathology. As shown in Figure
16 6c, PIH-AuNRs had no measurable adverse effects on liver function and immune system
17 throughout profiles. For example, 100 mg kg⁻¹ of PIH-AuNRs resulted in negligible
18 hepatotoxicity, and no obvious rise in levels of alanine transaminase (ALT), aspartate
19 transaminase (AST) and total bilirubin (TBIL) were observed. In addition, the inflammatory
20 cytokines, including tumor necrosis factor (TNF- α), Interleukin 1 beta (IL-1 β) and Interleukin 6
21 (IL-6), maintained at normal levels, demonstrating PIH-AuNRs have minimal adverse
22 immunogenicity.
23
24
25
26
27
28
29
30
31
32
33
34
35
36
37
38
39
40
41
42
43

44 After a 12-day treatment, mice in the PIH-AuNRs and control groups were sacrificed, and major
45 organs were harvested and imaged. We found that all organs in both groups showed similar size,
46 weight and texture, and particularly, no apparent difference in liver and spleen were observed
47 (Figure 6d). In addition, organ tissues were fixed and stained with hematoxylin and eosin, and no
48 pathological abnormalities, degenerations or lesions were detected in the PIH-AuNRs group.
49
50
51
52
53
54
55
56
57
58
59
60

1
2
3 Therefore, all these data indicate that PIH-AuNRs have good biocompatibility, and have the
4
5 great potential for the treatment of MERS in the clinic.
6
7

8 9 **Conclusion**

10
11
12 In this study, we have developed a novel gold nanorod-based HR1 peptide inhibitor (PIH-
13
14 AuNRs) for MERS. PIH is a potent HR1 inhibitor, and can selectively inhibit MERS-Cov S
15
16 protein-mediated cell fusion with IC_{50} of 1.171 μ M. Particularly, PIH-AuNRs exhibit ten-fold
17
18 higher inhibitory activity than PIH, and can completely inhibit cell fusion at 1.171 μ M. In
19
20 addition, PIH-AuNRs showed good biostability and biocompatibility *in vitro* and *in vivo*,
21
22 indicating that they have a broad application prospects for MERS treatment. Therefore, PIH-
23
24 AuNRs are a promising antiviral agent, and may have a huge impact on developing
25
26 pharmaceuticals in the clinic.
27
28
29
30
31
32
33
34
35
36
37
38
39
40
41
42
43
44
45
46
47
48
49
50
51
52
53
54
55
56
57
58
59
60

FIGURES

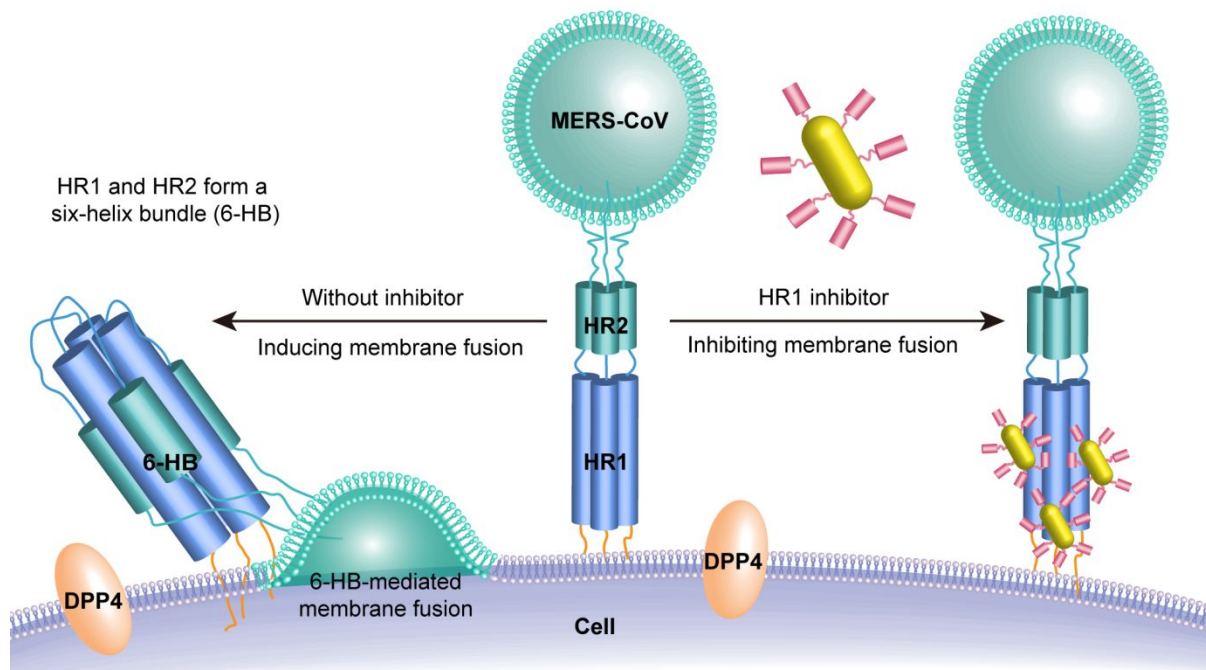


Figure 1. Schematic diagram of the inhibition of MERS-COV S2 subunit-mediated membrane fusion with HR1 inhibitors. HR1 inhibitor can inhibit HR1/HR2 complex (6-HB)-mediated membrane fusion, and prevent MERS-CoV infections.

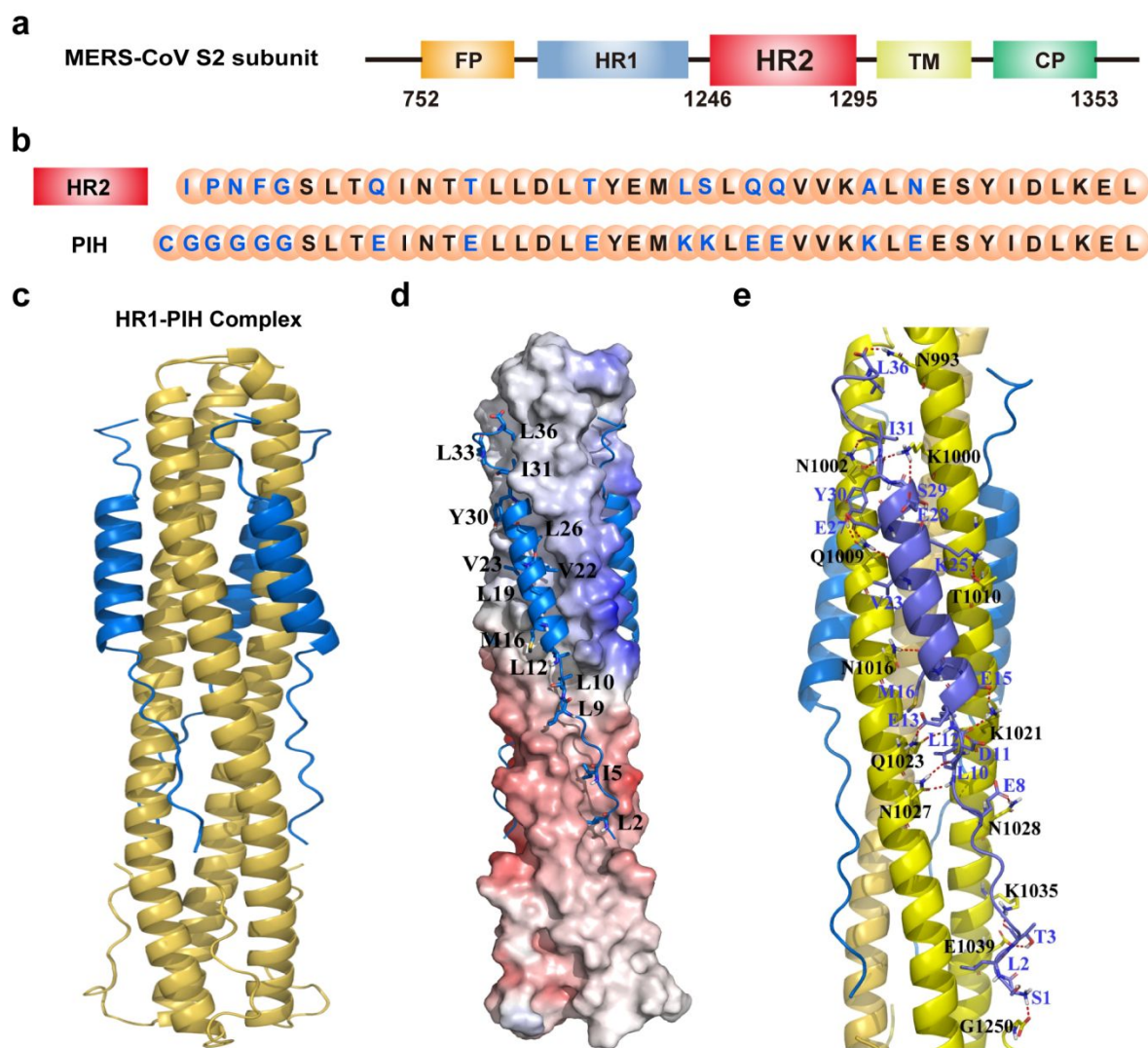


Figure 2. Design of HR1 peptide inhibitors. (a) Schematic representation of MERS-CoV S protein S2 subunit. FP, fusion peptide; HR1, heptad repeat 1 domain; HR2, heptad repeat 2 domain; TM, transmembrane domain; CP, cytoplasmic domain. (b) PIH was designed based on the sequence of HR2. (c) Overview of MERS-CoV-PIH complex structure. The core structures of MERS-CoV (HR1) and PIH are colored in yellow and blue, respectively. (d) Electrostatic potential surface of the central HR1 helices was calculated using PyMOL. The hydrophobic grooves are formed between each of two adjacent HR1 helices. PIH showed high binding affinity to the grooves. (e) PIH mimics the conformation of HR2 binding domain, and shows the strong

hydrophilic interactions with HR1 helices. The residues involved in the formation of hydrogen bonds are properly labeled, and hydrogen bonds are shown in red dashed lines.

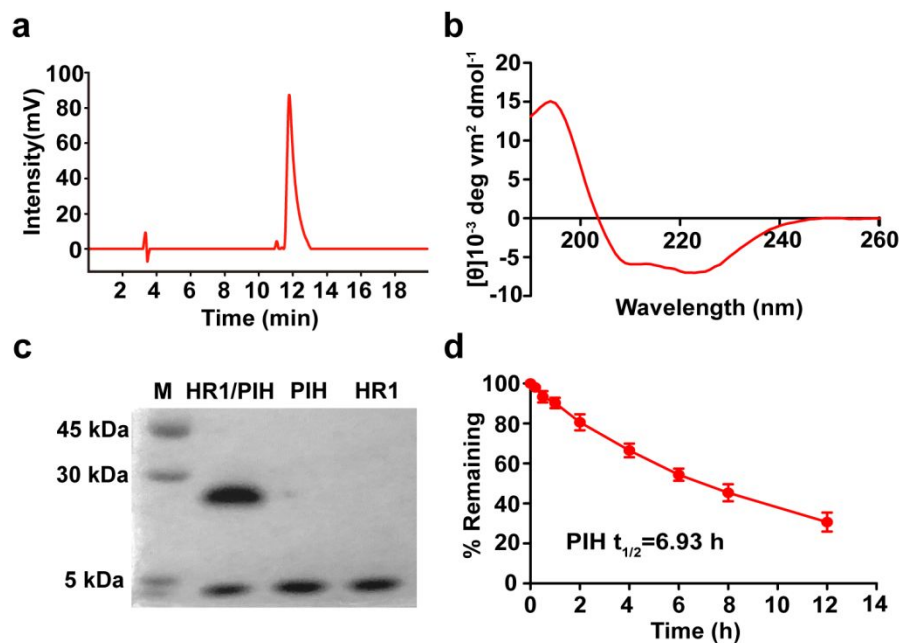


Figure 3. Synthesis and characterization of PIH. (a) The HPLC chromatogram of PIH. (b) The circular dichroism spectrum of PIH. PIH forms α -helix. (c) Determination of the 6-HB formation between HR1 and PIH by SDS-PAGE. (d) Serum stability of PIH. The data are expressed as means \pm s. d. (n=10).

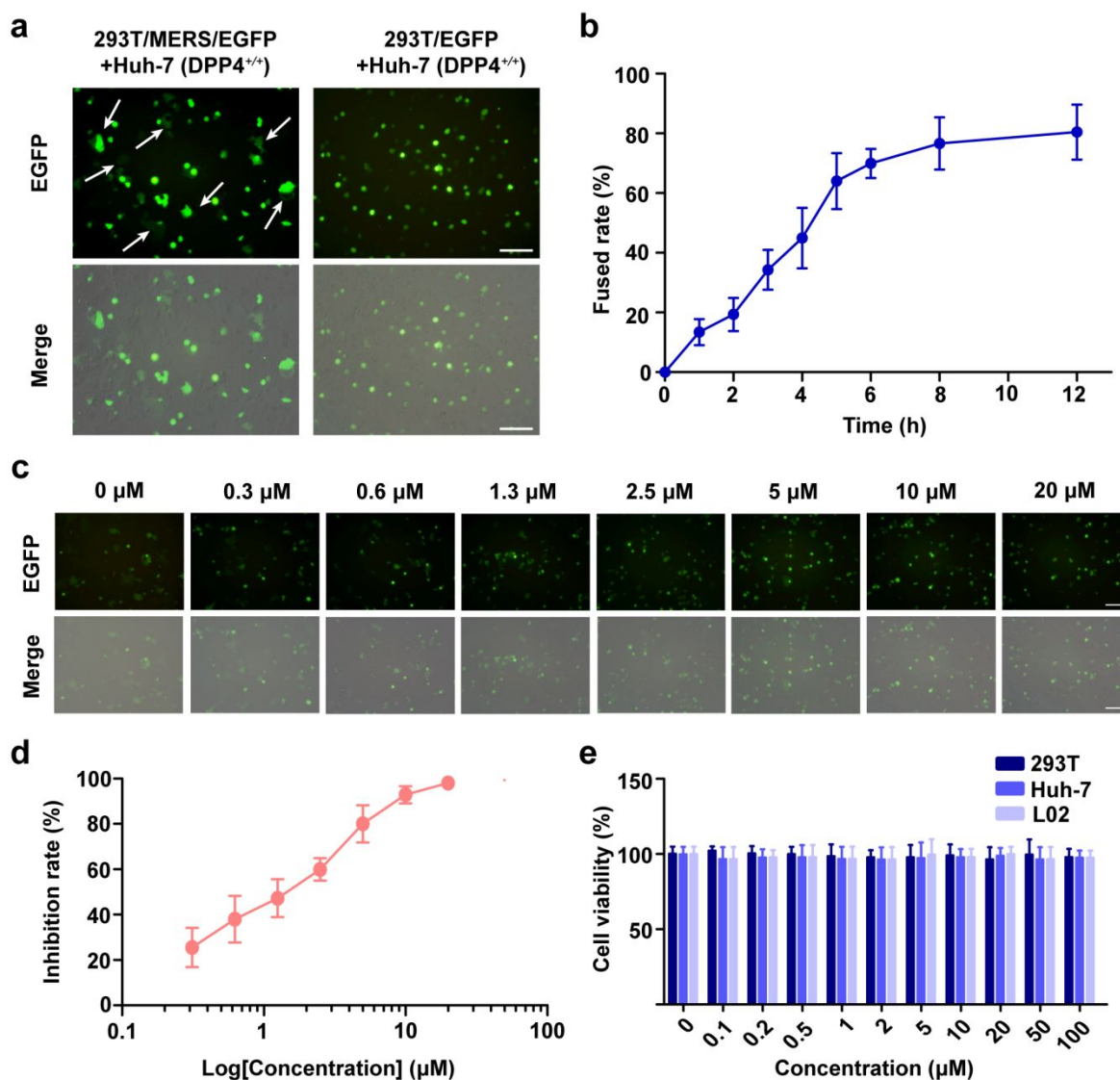


Figure 4. *In vitro* biological evaluation of PIH. (a) Representative fluorescent Images of cell fusion after 6-hour co-culture. The white arrows show the fused cells formed between 293T/MERS/EGFP cells and Huh-7 cells. Scale bars, 100 μ m. (b) Percentages of cell fusion at different time points. (c) Representative images of cell fusion in the presence of PIH. Scale bars, 100 μ m. (d) Inhibitory activity of PIH on MERS-CoV S2 subunit-mediated cell fusion. (e) The cytotoxicity of PIH against 293T, Huh-7 and L02 cells for 48 hours. The data are expressed as

means \pm s. d. (n=10).

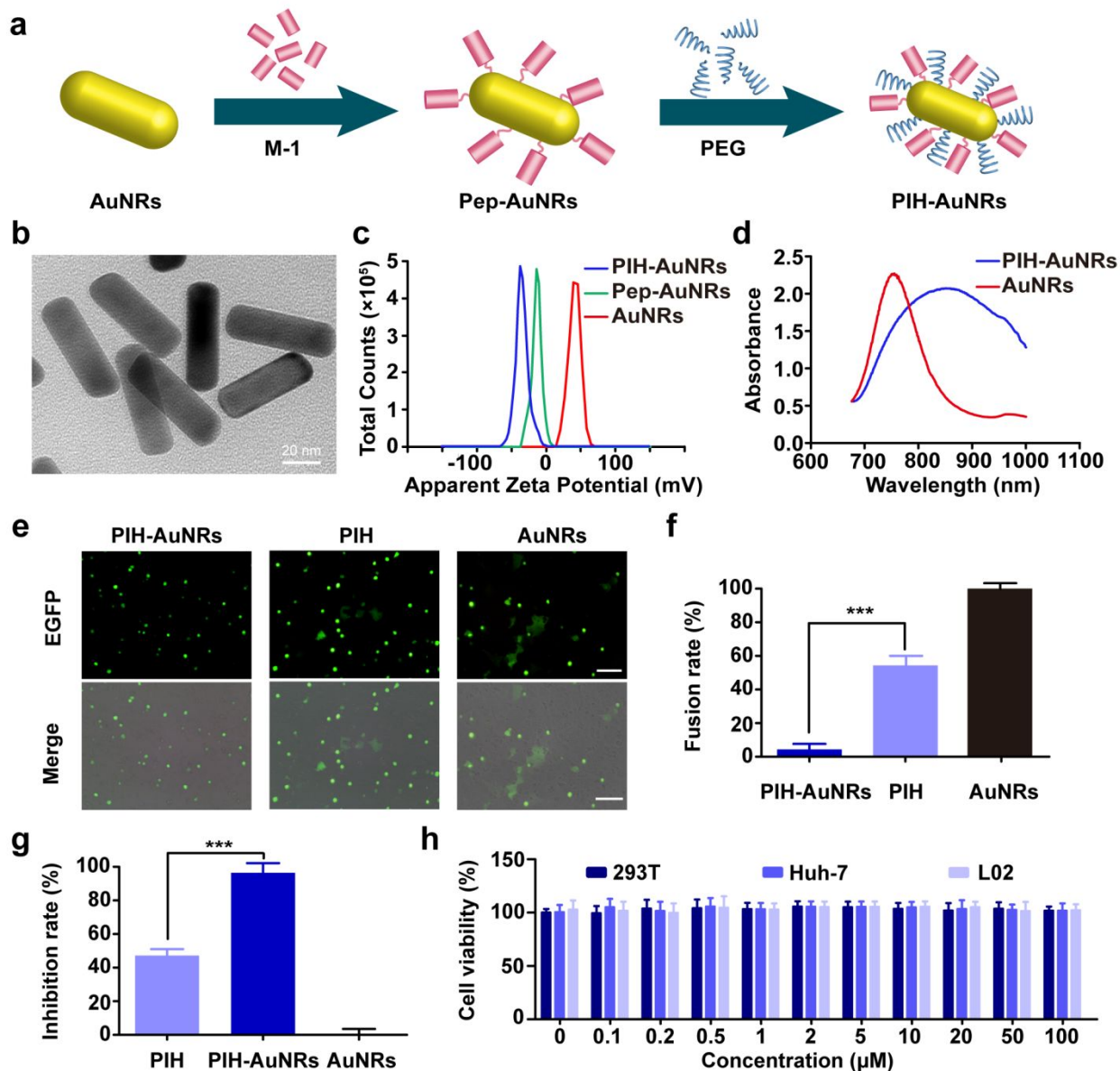


Figure 5. The preparation and characterization of PIH-AuNRs. (a) The preparation of PIH-AuNRs. (b) TEM images of PIH-AuNRs. Scale bar, 20 nm. (c) Zeta potential of AuNRs, Pep-AuNRs and PIH-AuNRs. (d) UV-Vis spectra of PIH-AuNRs and AuNRs. (e) Representative images of cell fusion in the presence of PIH, AuNRs and PIH-AuNRs. Scale bars, 100 μ m. (f) Quantification of cell fusion between Huh-7 and 293T/MERS/EGFP cells in the presence of PIH,

AuNRs and PIH-AuNRs. (g) Inhibitory activity of PIH-AuNRs on MERS-CoV S2 subunit-mediated cell fusion. *** represents $p < 0.001$. (h) The cytotoxicity of PIH-AuNRs against 293T, Huh-7 and L02 cells for 48 hours. The data are presented as means \pm s. d. (n=10).

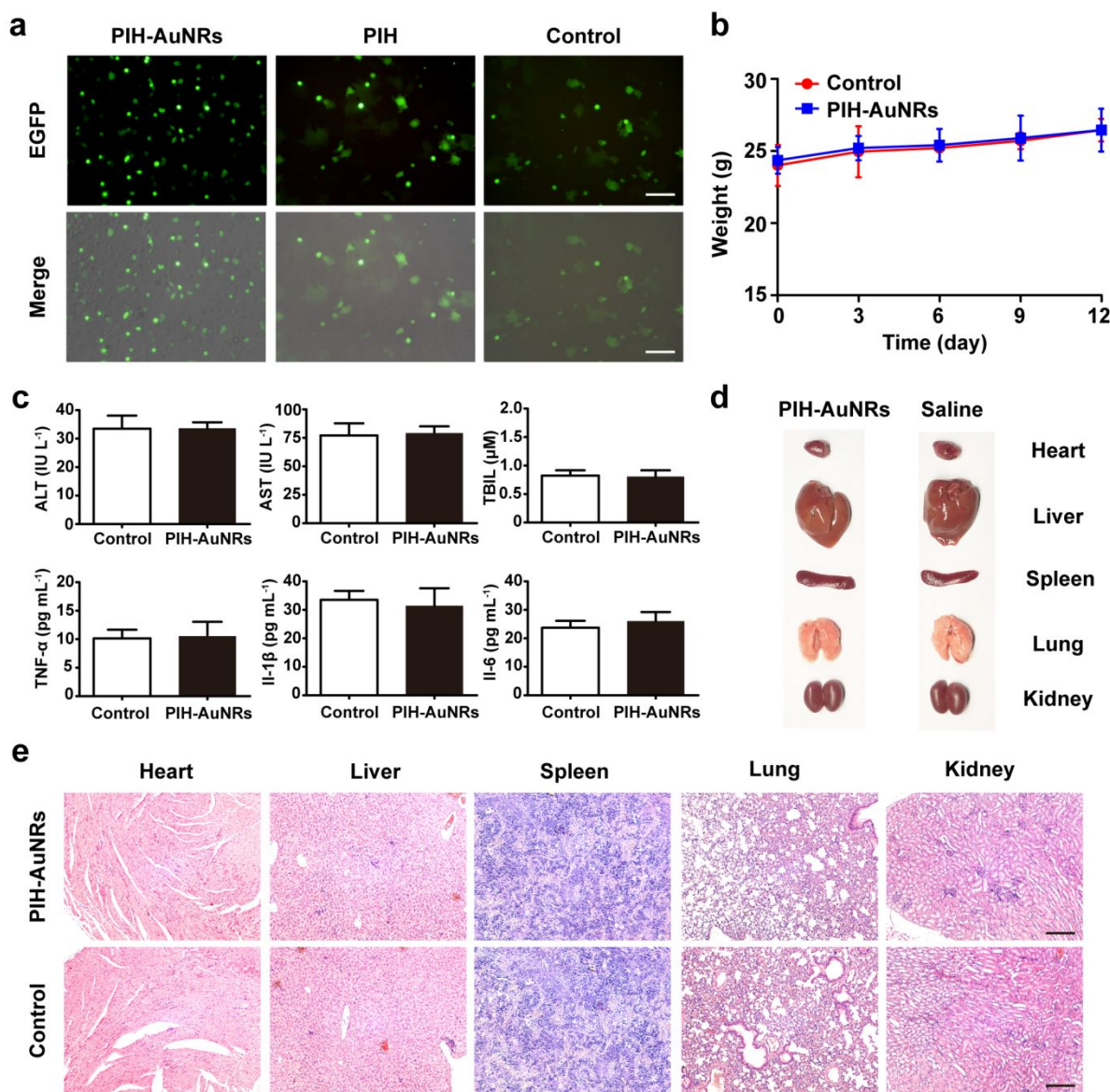


Figure 6. *In vitro* and *in vivo* biological evaluation of PIH-AuNRs. (a) Representative images of cell fusion in the presence of PIH, PIH-AuNRs and PBS, pre-incubated with serum for 12 hours. Scale bars, 100 μm. (b) Body weights of mice in the PIH-AuNRs group and control group. (c)

1
2
3 Biosafety evaluation of PIH-AuNRs in vivo. Liver functions (ALT, AST and TBIL) and
4 inflammatory cytokines (TNF- α , Il-1 β and Il-6) were measured by ELISA assays. (d)
5
6 Representative images of organs of mice in the PIH-AuNRs group and control group, including
7
8 heart, liver, spleen, lung and kidney. (e) H&E histopathological sections of tissues. The data are
9
10 presented as means \pm s. d. (n=10). Scale bars, 100 μ m.
11
12
13

14 15 ASSOCIATED CONTENT

16 17 18 **Supporting Information.**

19
20 The following files are available free of charge.
21
22

23
24 Sequences and docking scores of designed peptides, LC-ESI-MS of PIH, Native-PAGE analysis
25
26 of PIH, HPLC chromatograms of serum stability, original large fluorescence images of Figures 4,
27
28 5 and 6, HPLC chromatograms of the supernatant of the reaction mixture between PIH and
29
30 AuNRs. (doc)
31
32
33

34 35 AUTHOR INFORMATION

36 37 38 **Corresponding Author**

39
40 * E-mail: xning@nju.edu.cn (X. Ning)
41
42

43
44 * E-mail: qingj@nju.edu.cn (Q. Jiang)
45
46

47
48 * E-mail: zhangyu2007sm@163.com (Y. Zhang)
49
50

51 52 **Author Contributions**

53
54 #Xinyu Huang and Yadong Luo contributed equally to this work.
55
56
57
58
59
60

Notes

The authors declare no competing financial interest.

ACKNOWLEDGMENT

The works were supported by the National Key Research and Development Program of China (Grant No. 2018YFB1105400), the National Natural Science Foundation of China (Grant No. 21708019), the Thousand Talents Program for Young Researchers, the Natural Science Foundation of Jiangsu Province (Grant No. BK20180334), the Shuangchuang Program of Jiangsu Province, the Fundamental Research Funds for Central Universities Nanjing University and the Scientific Research Foundation of Graduate School of Nanjing University (Grant No. 2017ZDL04).

REFERENCES

- (1) Groot, R. J., De; Baker, S. C.; Baric, R. S.; Brown, C. S.; Christian, D.; Luis, E.; Fouchier, R. A. M.; Monica, G.; Gorbalenya, A. E.; Memish, Z. A. Middle East Respiratory Syndrome Coronavirus (MERS-CoV): Announcement of the Coronavirus Study Group. *J. Virol.* **2013**, *87*, 7790-7792.
- (2) Abdullah, A.; Allison, M.; Trish M, P.; Connie S, P.; Abdullah A, A. R.; Derek A T, C.; Zaki N, A.; Maher, A.; Abdulmohsen, A.; Hatem, M. Hospital Outbreak of Middle East Respiratory Syndrome Coronavirus. *N. Engl. J. Med.* **2013**, *369*, 407-416.
- (3) Memish, Z. A.; Zumla, A. I.; Abdullah, A. Middle East Respiratory Syndrome Coronavirus Infections in Health Care Workers. *N. Engl. J. Med.* **2013**, *369*, 884-886.
- (4) Zaki, A. M.; van Boheemen, S.; Bestebroer, T. M.; Osterhaus, A. D.; Fouchier, R. A. Isolation of a Novel Coronavirus from a Man with Pneumonia in Saudi Arabia. *N. Engl. J. Med.* **2012**, *367*, 1814-1820.

- 1
2
3 (5) Assiri, A.; Al-Tawfiq, J. A.; Al-Rabeeah, A. A.; Al-Rabiah, F. A.; Al-Hajjar, S.; Al-Barrak,
4 A.; Flemban, H.; Al-Nassir, W. N.; Balkhy, H. H.; Al-Hakeem, R. F. Epidemiological,
5 Demographic, and Clinical Characteristics of 47 cases of Middle East Respiratory Syndrome
6 Coronavirus Disease from Saudi Arabia: a Descriptive Study. *Lancet Infect. Dis.* **2013**, *13*, 752-
7 761.
8
9
10
11
12
13
14 (6) Chan, J. F. W.; Lau, S. K. P.; To, K. K. W.; Cheng, V. C. C.; Woo, P. C. Y.; Kwok-Yung, Y.
15 Middle East Respiratory Syndrome Coronavirus: Another Zoonotic Betacoronavirus Causing
16 SARS-like Disease. *Clin. Microbiol. Rev.* **2015**, *28*, 465-522.
17
18
19
20
21 (7) Leung, C. H. C.; Gomersall, C. D. Middle East Respiratory Syndrome. *Intensive Care Med.*
22 **2014**, *40*, 1015-1017.
23
24
25
26 (8) Al-Tawfiq, J. A.; Momattin, H.; Dib, J.; Memish, Z. A. Ribavirin and Interferon Therapy in
27 Patients Infected with the Middle East Respiratory Syndrome Coronavirus: an Observational
28 Study. *Int. J. Infect. Dis.* **2014**, *20*, 42-46.
29
30
31
32
33 (9) Omrani, A. S.; Saad, M. M.; Kamran, B.; Abdelkarim, B.; Mohammed, A. M.; Alaidaroos, A.
34 Y.; Almakhlafi, G. A.; Albarrak, M. M.; Memish, Z. A.; Albarrak, A. M. Ribavirin and
35 Interferon Alfa-2a for Severe Middle East Respiratory Syndrome Coronavirus Infection: a
36 Retrospective Cohort Study. *Lancet Infect. Dis.* **2014**, *14*, 1090-1095.
37
38
39
40
41
42 (10) Shalhoub, S.; Farahat, F.; Al-Jiffri, A.; Simhairi, R.; Shamma, O.; Siddiqi, N.; Mushtaq, A.
43 IFN-alpha2a or IFN-beta1a in Combination with Ribavirin to Treat Middle East Respiratory
44 Syndrome Coronavirus Pneumonia: a Retrospective Study. *J. Antimicrob. Chemother.* **2015**, *70*,
45 2129-2132.
46
47
48
49
50
51
52
53
54
55
56
57
58
59
60

1
2
3 (11) Yuan, Y.; Cao, D.; Zhang, Y.; Ma, J.; Qi, J.; Wang, Q.; Lu, G.; Wu, Y.; Yan, J.; Shi, Y.;
4 Zhang, X.; Gao, G. F. Cryo-EM Structures of MERS-CoV and SARS-CoV Spike Glycoproteins
5 Reveal the Dynamic Receptor Binding Domains. *Nat. Commun.* **2017**, *8*, 15092.
6
7

8
9
10 (12) Stefanie, G.; Stephanie, B.; Franziska, K.; Florian, W.; Adeline, H.; Annika, K. M. K.;
11 Kathrin, W.; Michael, W.; Benjamin, M.; Christian, D., The Spike Protein of the Emerging
12 Betacoronavirus EMC Uses a Novel Coronavirus Receptor for Entry, Can be Activated by
13 TMPRSS2, and is Targeted by Neutralizing Antibodies. *J. Virol.* **2013**, *87*, 5502-5511.
14
15
16

17
18 (13) Raj, V. S.; Mou, H.; Smits, S. L.; Dekkers, D. H.; Muller, M. A.; Dijkman, R.; Muth, D.;
19 Demmers, J. A.; Zaki, A.; Fouchier, R. A.; Thiel, V.; Drosten, C.; Rottier, P. J.; Osterhaus, A.
20 D.; Bosch, B. J.; Haagmans, B. L. Dipeptidyl Peptidase 4 is a Functional Receptor for the
21 Emerging Human Coronavirus-EMC. *Nature* **2013**, *495*, 251-254.
22
23
24
25

26
27 (14) Gao, J.; Lu, G.; Qi, J.; Li, Y.; Wu, Y.; Deng, Y.; Geng, H.; Li, H.; Wang, Q.; Xiao, H.; Tan,
28 W.; Yan, J.; Gao, G. F. Structure of the Fusion Core and Inhibition of Fusion by a Heptad Repeat
29 Peptide Derived from the S Protein of Middle East Respiratory Syndrome Coronavirus. *J. Virol.*
30 **2013**, *87*, 13134-13140.
31
32
33
34

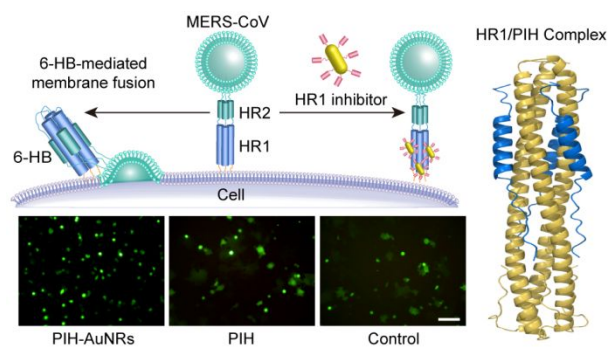
35
36 (15) Merrifield, R. B. Solid Phase Peptide Synthesis. I. The Synthesis of a Tetrapeptide. *J. Am.*
37 *Chem. Soc.* **1963**, *85*, 2149-2154.
38
39
40
41

42 (16) Bosch, B. J.; van der Zee, R.; de Haan, C. A.; Rottier, P. J. The Coronavirus Spike Protein is
43 a Class I Virus Fusion Protein: Structural and Functional Characterization of the Fusion Core
44 Complex. *J. Virol.* **2013**, *77*, 8801-8811.
45
46
47
48

49 (17) Tripet, B.; Howard, M. W.; Jobling, M.; Holmes, R. K.; Holmes, K. V.; Hodges, R. S.
50 Structural Characterization of the SARS-coronavirus Spike S Fusion Protein Core. *J. Biol. Chem.*
51 **2004**, *279*, 20836-20849.
52
53
54
55

- 1
2
3 (18) Fosgerau, K.; Hoffmann, T. Peptide Therapeutics: Current Status and Future Directions.
4
5 *Drug Discov. Today* **2015**, *20*, 122-128.
6
7
8 (19) Chan, F. W.; Chan, K. H.; Choi, K. Y.; To, K. W.; Tse, H.; Cai, J. P.; Yeung, M. L.; Cheng,
9
10 V. C.; Chen, H.; Che, X. Y.; Lau, K. P. Differential Cell Line Susceptibility to the Emerging
11
12 Novel Human Betacoronavirus 2c EMC/2012: Implications for Disease Pathogenesis and
13
14 Clinical Manifestation. *J. Infect. Dis.* **2013**, *207*, 1743-1752.
15
16
17 (20) Lu, L.; Liu, Q.; Zhu, Y.; Chan, K. H.; Qin, L.; Li, Y.; Wang, Q.; Chan, J. F.; Du, L.; Yu, F.;
18
19 Ma, C.; Ye, S.; Yuen, K. Y.; Zhang, R.; Jiang, S. Structure-based Discovery of Middle East
20
21 Respiratory Syndrome Coronavirus Fusion Inhibitor. *Nat. Commun.* **2014**, *5*, 3067.
22
23
24 (21) HãVard, J.; Pamela, H.; Hancock, R. E. W. Peptide Antimicrobial Agents. *Clin. Microbiol.*
25
26 *Rev.* **2006**, *19*, 491-511.
27
28
29 (22) Kaspar, A. A.; Reichert, J. M. Future Directions for Peptide Therapeutics Development.
30
31 *Drug Discov. Today* **2013**, *18*, 807-817.
32
33
34 (23) Chakravarthy, K. V.; Bonoiu, A. C.; Davis, W. G.; Ranjan, P.; Ding, H.; Hu, R.; Bowzard,
35
36 J. B.; Bergey, E. J.; Katz, J. M.; Knight, P. R.; Sambhara, S.; Prasad, P. N. Gold Nanorod
37
38 Delivery of an ssRNA Immune Activator Inhibits Pandemic H1N1 Influenza Viral
39
40 Replication. *Proc. Natl. Acad. Sci. U. S. A.* **2010**, *107*, 10172-10177.
41
42
43 (24) Yucai, W.; Black, K. C. L.; Hannah, L.; Weiyang, L.; Yu, Z.; Xin, C.; Dehui, W.; Si-Yun,
44
45 L.; Max, L.; Paul, K. Comparison Study of Gold Nanohexapods, Nanorods, and Nanocages for
46
47 Photothermal Cancer Treatment. *ACS Nano* **2013**, *7*, 2068-2077.
48
49
50 (25) Yan, E.; Cao, M.; Wang, Y.; Hao, X.; Pei, S.; Gao, J.; Wang, Y.; Zhang, Z.; Zhang, D. Gold
51
52 Nanorods Contained Polyvinyl Alcohol/Chitosan Nanofiber Matrix for Cell Imaging and Drug
53
54 Delivery. *Mater. Sci. Eng., C* **2016**, *58*, 1090.
55
56
57
58
59
60

- 1
2
3 (26) Ming, Z.; Xueying, H. Nanoparticles Comprising a Mixed Monolayer for Specific Bindings
4 with Biomolecules. *J. Am. Chem. Soc.* **2004**, *126*, 12047-12054.
5
6
7 (27) Moghimi, S. M.; Patel, H. M. Serum-mediated Recognition of Liposomes by Phagocytic
8 Cells of the Reticuloendothelial System – The Concept of Tissue Specificity. *Adv. Drug Delivery*
9 *Rev.* **1998**, *32*, 45-60.
10
11 (28) Papisov, M. I. Theoretical Considerations of RES-avoiding Liposomes: Molecular
12 Mechanics and Chemistry of Liposome Interactions. *Adv. Drug Delivery Rev.* **1998**, *32*, 119-138.
13
14 (29) Wan-Seob, C.; Minjung, C.; Jinyoung, J.; Mina, C.; Hea-Young, C.; Beom Seok, H.; Sheen
15 Hee, K.; Hyoung Ook, K.; Taik, L. Y.; Bong Hyun, C. Acute Toxicity and Pharmacokinetics of
16 13 nm-sized PEG-coated Gold Nanoparticles. *Toxicol. Appl. Pharmacol.* **2009**, *236*, 16-24.
17
18 (30) Libutti, S. K.; Paciotti, G. F.; Byrnes, A. A.; Alexander, H. R., Jr.; Gannon, W. E.; Walker,
19 M.; Seidel, G. D.; Yuldasheva, N.; Tamarkin, L. Phase I and Pharmacokinetic Studies of CYT-
20 6091, a Novel PEGylated Colloidal Gold-rhTNF Nanomedicine. *Clin. Cancer Res.* **2010**, *16*,
21 6139-6149.
22
23 (31) Balasubramanian, S. K.; Jittiwat, J.; Manikandan, J.; Ong, C. N.; Yu, L. E.; Ong, W. Y.
24 Biodistribution of Gold Nanoparticles and Gene Expression Changes in the Liver and Spleen
25 after Intravenous Administration in Rats. *Biomaterials* **2010**, *31*, 2034-2042.
26
27 (32) Jong, W. H. D.; Hagens, W. I.; Krystek, P.; Burger, M. C.; Sips, A. J. A. M.; Geertsma, R.
28 E. Particle Size-dependent Organ Distribution of Gold Nanoparticles after Intravenous
29 Administration. *Biomaterials* **2008**, *29*, 1912-1919.
30
31
32
33
34
35
36
37
38
39
40
41
42
43
44
45
46
47
48
49
50
51
52
53
54
55
56
57
58
59
60



For Table of Contents Only